particles

MDPI

Article

The Study and Development of BPM Noise Monitoring at the Siam Photon Source

Wanisa Promdee [1,*], Sukho Kongtawong [1,*], Surakawin Suebka [1,*], Thapakron Pulampong [1], Natthawut Suradet [1], Roengrut Rujanakraikarn [1], Puttimate Hirunuran [2] and Siriwan Jummunt [1]

[1] Synchrotron Light Research Institute, Muang District, Nakhon Ratchasima 30000, Thailand; thapakron@slri.or.th (T.P.); natthawuts@slri.or.th (N.S.); roengrut@slri.or.th (R.R.); siriwan@slri.or.th (S.J.)
[2] Big Data Institute, Chatuchak, Bangkok 10900, Thailand; gyed43@gmail.com
* Correspondence: wanisa@slri.or.th (W.P.); sukho@slri.or.th (S.K.); surakawin@slri.or.th (S.S.)

Abstract

This study presents the development of a noise-monitoring system for the storage ring at the Siam Photon Source, designed to detect and classify noise patterns in real time using beam position monitor (BPM) data. Noise patterns were categorized into four classes: broad peak, multipeak, normal peak, and no beam. Two BPMs located at the multipole wiggler section, BPM-MPW1 and BPM-MPW2, were selected for detailed monitoring based on consistent noise trends observed across the ring. The dataset was organized in two complementary formats: two-dimensional (2D) images used for training and validating the models and one-dimensional (1D) CSV files containing the corresponding raw numerical signal data. Pre-trained deep learning and 1D convolutional neural network (CNN) models were employed to classify these patterns, achieving an overall classification accuracy of up to 99.83%. The system integrates with the EPICS control framework and archiver log data, enabling continuous data acquisition and long-term analyses. Visualization and monitoring features were developed using CS-Studio/Phoebus, providing both operators and beamline scientists with intuitive tools to track beam quality and investigate noise-related anomalies. This approach highlights the potential of combining beam diagnostics with machine learning to enhance operational stability and optimize the synchrotron radiation performance for user experiments.

Keywords: beam diagnostic; noise monitoring; machine learning; EPICS

check for updates

Academic Editor: Hideaki Ohgaki

Received: 30 June 2025
Revised: 13 August 2025
Accepted: 20 August 2025
Published: 25 August 2025

Citation: Promdee, W.; Kongtawong, S.; Suebka, S.; Pulampong, T.; Suradet, N.; Rujanakraikarn, R.; Hirunuran, P.; Jummunt, S. The Study and Development of BPM Noise Monitoring at the Siam Photon Source. *Particles* **2025**, *8*, 76. https://doi.org/10.3390/particles8030076

Copyright: © 2025 by the authors. Licensee MDPI, Basel, Switzerland. This article is an open access article distributed under the terms and conditions of the Creative Commons Attribution (CC BY) license (https://creativecommons.org/licenses/by/4.0/).

1. Introduction

The Siam Photon Source (SPS) is a synchrotron light facility in Thailand that has been providing synchrotron radiation for multidisciplinary research and industrial applications for nearly three decades. The machine operates at a beam energy of 1.2 GeV and comprises a linear accelerator, booster synchrotron, and storage ring. To ensure a high beam quality and operational stability, the ongoing development and enhancement of beam diagnostic systems remain a central focus of the facility.

Beam diagnostics at SPS [1] are employed to monitor fundamental beam parameters, including the position, size, and intensity. These measurements are crucial for ensuring optimal beam performance, enabling real-time feedback and corrections, and supporting machine studies and upgrades. One of the persistent challenges in synchrotron operations is beam noise [2], which can originate from various sources, such as magnet power supply fluctuations, mechanical vibrations, thermal instabilities, and electronic interference. These

noise sources can compromise beam stability, impact the experimental precision, and reduce the overall machine performance. The accurate identification and classification of such noise are therefore essential for effective mitigation and system optimization.

The beam position monitor (BPM) is an essential beam diagnostic tool used to monitor and measure beam position and orbit/trajectory. Moreover, it can be employed to analyze noise in the electron beam position [3]. At the Siam Photon Source (SPS), 26 BPM buttons are distributed around the storage ring. Two types of BPM processors have been installed: analog and digital, specifically Bergoz Multiplexed Beam Position Monitors (MX-BPMs) [4] and the Libera Spark ERXR (eBPM) [5]. The MX-BPMs are primarily used for slow orbit feedback (SOFB) in the storage ring; however, for digital data acquisition aimed at noise analyses, only the six BPM pick-ups associated with the insertion devices are utilized. In particular, the BPMs located upstream (BPM-MPW1) and downstream (BPM-MPW2) of the multipole wiggler as seen in Figure 1 were selected for this study.

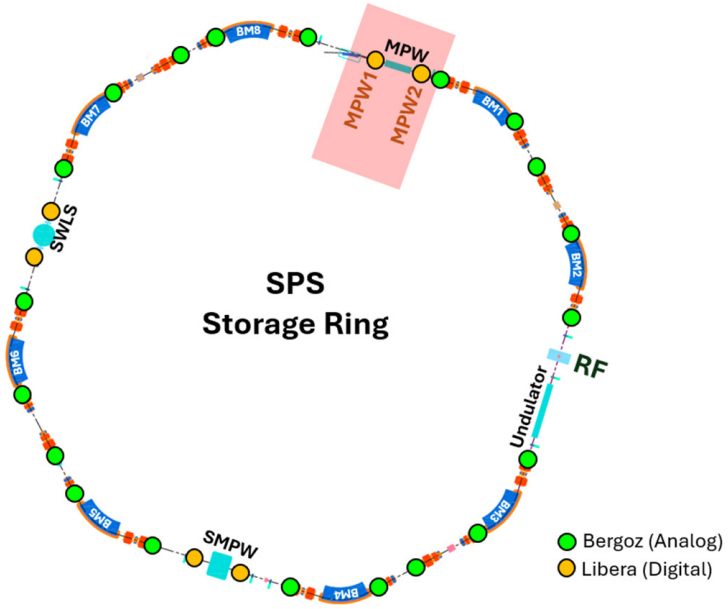
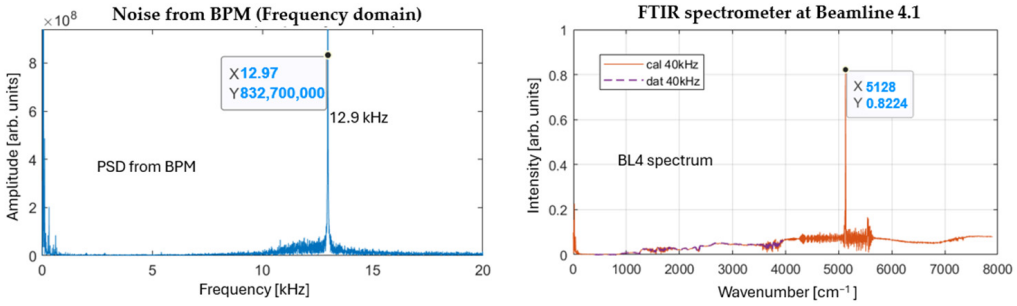


Figure 1. Beam position monitor (BPM) layout of the Siam Photon Source. BPM-MPW1 and BPM-MPW2, located in the clockwise direction, are highlighted in red.

Noise originating from the electron beam was measured using beam position monitor (BPM) pick-ups installed in the storage ring. It was observed that vibrations in the horizontal and vertical beam positions, as recorded by the digital BPM processor (see Figure 2a), are correlated with noise spikes detected by a Fourier transform infrared (FTIR) spectrometer at Beamline 4.1: Infrared Spectroscopy and Imaging. This correlation is based on measurement data acquired at the experimental end station, as shown in Figure 2b. When the sharp frequency becomes broadened, it can adversely affect the experimental results in the infrared range by distorting the spectral features associated with the molecular vibrational modes of the samples under investigation. Consequently, this distortion can hinder the accurate interpretation of the measured data.



(**a**) (**b**)

Figure 2. The spectrum of the signals: (**a**) noise data detected from beam position monitor and (**b**) spectrum measured from a sample at end station of Beamline 4.1.

In addition, distinct peaks were observed in the spectrum of the forward signal from the RF system, whose positions varied with changes in the RF voltage, as seen in Figure 3. This behavior is related to the synchrotron frequency [6], as described by Equation (1):

$$\omega_s = \omega_0 \sqrt{\frac{ehV_{rf}\alpha_c cos\Psi_s}{2\pi E}}, \tag{1}$$

where ω_0 is the revolution angular frequency, e is the elementary charge, h is the harmonic number, V_{rf} is the RF voltage, α_c is the momentum compaction factor, Ψ_s is the synchronous phase, and E is the beam energy.

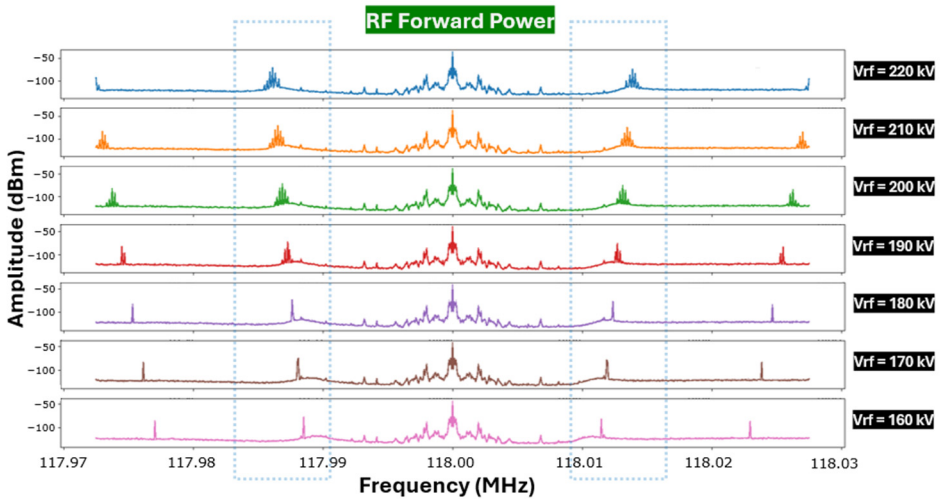


Figure 3. Spectrum of forward power at the diagnostic port of the low-level RF (LLRF) when varying the RF voltage from 220 kV to 160 kV. The frequency shift is highlighted by the dotted blue boxes.

This study proposes the development of a noise-monitoring system that leverages machine learning techniques to analyze noise patterns derived from electron beam position data. The system is designed to detect and classify noise into four categories by employing various data-preparation methods and machine learning algorithms. The dataset was collected in two formats: one-dimensional (1D) numerical data and two-dimensional (2D) images. The results obtained from these two data types were compared to evaluate their effectiveness in classification performance. Integration with the EPICS control system [7] facilitates real-time data acquisition, thereby enhancing the operational responsiveness. Furthermore, a dedicated graphical user interface (GUI) developed using

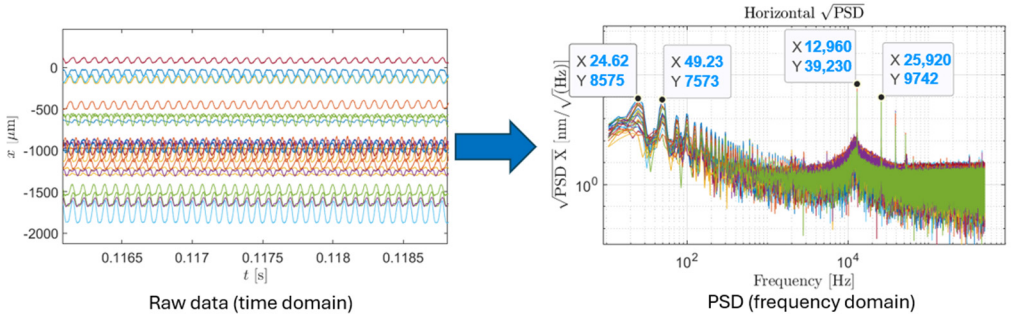
CS-Studio/Phoebus [8] provides operators with intuitive tools for monitoring, visualization, and system interaction.

2. Materials and Methods

This section describes the setup of the noise-monitoring system implemented at the Siam Photon Source. The process began with the acquisition and analysis of noise signals, followed by the labeling and classification of noise types and the training of machine learning models using the data collected from BPM processors. Subsequently, the entire system was integrated into the control infrastructure using the EPICS framework and visualized through a dedicated interface developed in CS-Studio/Phoebus.

2.1. Noise Analysis

Noise Vibration readings from the position of electron beams can be detected using digital beam position monitors [3,9,10]. In this study, horizontal (X) and vertical (Y) positions were acquired as turn-by-turn data [11] from a Libera Spark ERXR processor [5] and subsequently analyzed using the power spectral density (PSD) technique, as seen in Figure 4. The BPM processor provided TBT signals via a direct SSH connection, which was accessed by a Python 3.9 script that remotely executed commands and retrieved the corresponding data. The horizontal and vertical positions in this study were obtained directly from the BPM processor to ensure a high temporal resolution and improved data fidelity.



(**a**) (**b**)

Figure 4. Example data from Libera Spark ERXR for all 26 BPMs shown in different colors: (**a**) raw data and (**b**) power spectral density (PSD).

To analyze the frequency characteristics of beam noise, we employed the Welch method [12] for estimating the PSD of the TBT data. The Welch PSD estimate $\hat{P}_{xx}(f)$ is given by the following:

$$\hat{P}_{xx}(f) = \frac{1}{K}\sum_{K=1}^{K}\frac{1}{U}\left|\sum_{n=0}^{N-1} x_k(n)\omega(n)e^{-j2\pi fn}\right|^2 \quad (2)$$

where K is overlapping segments, $x_k(n)$ is the data segment of length N, $\omega(n)$ is the window function, and U is the normalization factor defined by $U = \frac{1}{N}\sum_{n=0}^{N-1}\omega^2(n)$.

The Welch method improves the variance of the PSD estimate by dividing the time series data into overlapping segments, applying a window function to each segment (K), and averaging the resulting periodograms. Specifically, for each segment, the discrete Fourier transform (DFT) is calculated, and the squared magnitude is scaled to produce an estimate of the power distribution across frequencies. The average of these estimates then forms the final PSD, providing a smoother and more reliable spectrum compared to a single periodogram.

Practically, the PSD was computed using the scipy.signal.welch function from the SciPy library in Python. After generating the full-range PSD from the turn-by-turn data, the analysis focused on a specific frequency band of interest. In this study, attention was directed toward the noise component near 13 kHz, where a prominent peak was observed at an RF voltage (V_{rf}) of 200 kV. To account for shifts in the peak position when the RF voltage was reduced to 160 kV, a frequency span of approximately 3 kHz centered around 13 kHz was selected. This targeted frequency band ensured that variations in the synchrotron frequency induced by changes in the RF voltage were fully captured in the subsequent analysis.

2.2. Noise Classification and Learning

The noise patterns analyzed in the position readings of the electron beams were categorized into four distinct classes. These classes were subsequently labeled and used to train a machine learning model for predictive analyses.

2.2.1. Noise Labeling and Classification

From the investigation, the noise patterns were manually classified into four main types: broad, multipeak, normal peak, and no beam (off), as illustrated in Figure 5. In the classification results, the yellow label represents signals exhibiting multiple frequency components (multipeak). The green label corresponds to normal signals characterized by a single prominent spectral peak. The red label indicates cases where the frequency spectrum becomes broadened, suggesting a spread in the dominant noise frequency. Finally, the off state denotes periods when the beam is absent, and no significant spectral features are observed.

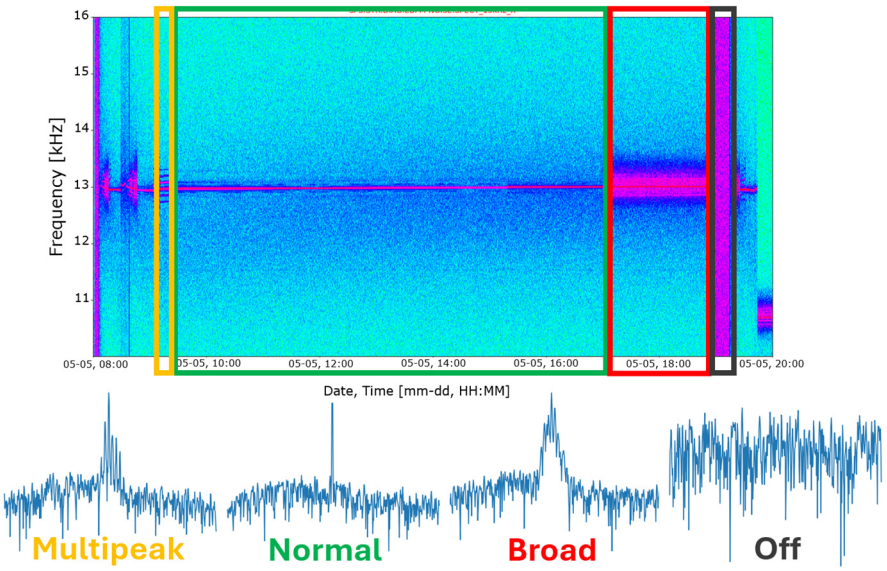


Figure 5. Examples of noise patterns during one operation shift. Yellow indicates multiple peaks, green indicates a narrow peak, red indicates a broad peak, and dark gray indicates no peak.

The labeling process involved selecting specific time ranges to extract and categorize the corresponding signal segments. These signals were manually classified by plotting and saving them as figures in .png format, followed by a visual inspection to determine their noise characteristics. Each noise figure was then moved to the appropriate class folder to be used as input for model training. The dataset was prepared in two formats: two-dimensional (2D) images for model input and one-dimensional (1D) CSV files containing the raw numerical data.

To reduce the time required for manual labeling, a previously trained prediction model was also used to perform a preliminary automatic classification of the noise patterns. The predicted results were then reviewed and manually verified before transferring the correctly labeled data into the training folder for subsequent machine learning.

2.2.2. Machine Learning Approaches

The aim of the machine learning method was to develop models capable of distinguishing between different noise types based on spectral features, thereby enhancing the monitoring system's ability to detect and interpret beam-related anomalies in real time. Two data representations were investigated to assess their impact on the classification performance: one-dimensional (1D) spectral vectors and two-dimensional (2D) spectrogram images, as seen in Figure 6.

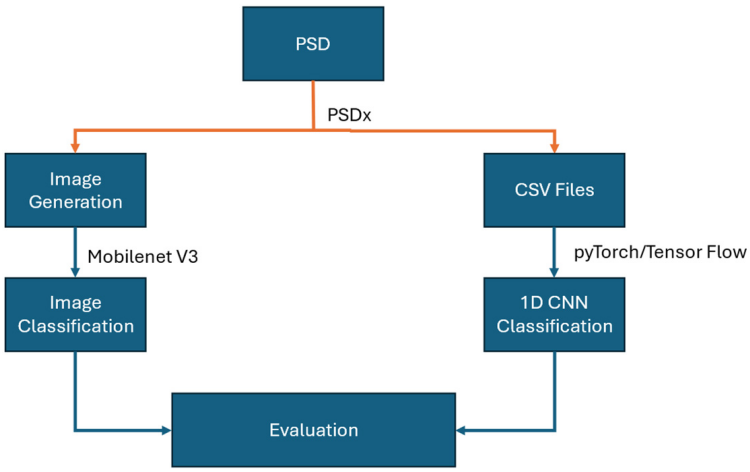


Figure 6. Diagram of the machine learning workflow for noise classification.

The dataset of each classified type was split into 70 percent for training and 30 percent for validation using stratified sampling to preserve the class balance. The 1D spectral vectors were used to train a custom 1D convolutional neural network (CNN) [13] built with TensorFlow 2.19.0 and PyTorch 2.7.1 [14], which included Conv1D, MaxPooling1D, and dense layers. For the 2D spectrogram images, transfer learning was applied by adapting the pre-trained MobileNetV3 model [15], replacing its final layers with a new classifier tailored to the four noise classes.

The models were trained using the Adam optimizer [16] and categorical cross-entropy loss, with early stopping applied (patience of 10 epochs) to reduce overfitting. A performance evaluation was conducted on the validation set using metrics such as the accuracy, precision, recall, and F1-score to comprehensively assess the model effectiveness.

2.3. Noise Monitoring

After developing the model to predict noise patterns, it was then applied to the real-time monitoring system. To implement this, the data from the BPM must first be analyzed and subsequently processed for decision-making. This process requires a trigger mechanism to initiate both data acquisition from the BPM and execution of the noise-prediction routine.

The overall noise-monitoring system is illustrated schematically in Figure 7. The system will be integrated into the EPICS framework [7], which serves as the control system for coordinating data acquisition and system management. To ensure consistent data logging with timestamps, each process variable (PV) must follow a standardized naming convention [17], structured as follows: <name of machine>:<location of

the system>:<system>:<instrument>:<function>. For example, the PV tag for logging the noise component around 13 kHz could be defined as follows: SPS:STR:DIAG:EBPM-NOISE:SPECT_13kHz_X, where

- SPS: Siam Photon Source;
- STR: storage ring;
- DIAG: beam diagnostics;
- EBPM-NOISE: PSD of the signals from digital BPM;
- SPECT_13kHz_X: spectrum around 13 kHz of the horizontal plane.

Once the PV was assigned, the EPICS Archiver Appliance [18] was employed to continuously store the logged process variable with its associated timestamps into a time-series database, making it possible to retrieve and review historical data when required. This functionality enables users to check the status of the tagged parameters.

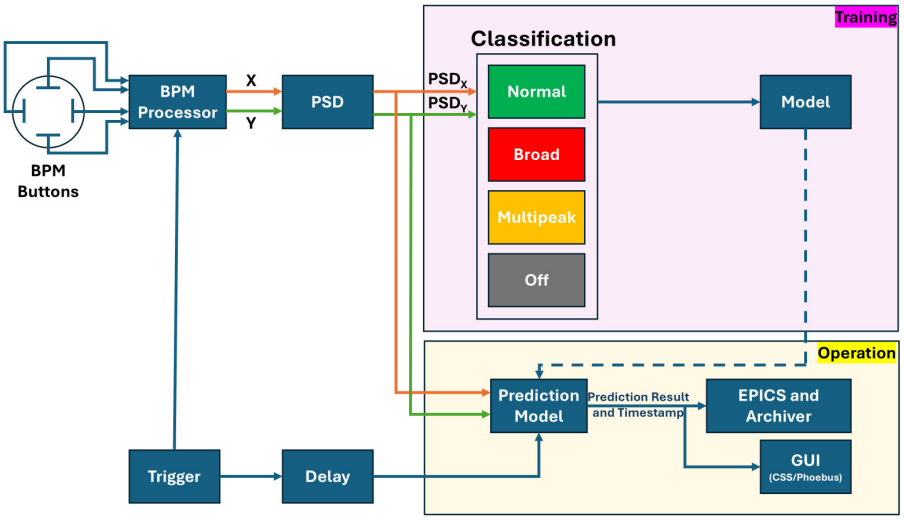


Figure 7. Schematic of noise-monitoring system at Siam Photon Source.

As illustrated in Figure 8, CS-Studio/Phoebus [8] was employed to provide an intuitive graphical user interface (GUI) for monitoring the signals. It is an open-source suite of tools designed for control system visualization and operation. It offers a flexible and highly customizable interface that allows operators and researchers to create real-time dashboards, trend plots, synoptic displays, and alarm panels. In this study, CS-Studio/Phoebus served as the front-end application integrated with the EPICS control system, enabling users to easily visualize noise data, track trends over time, and interact with the underlying PVs.

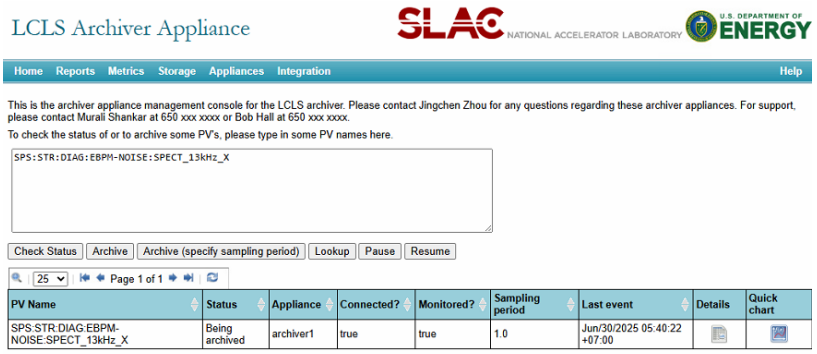


Figure 8. The EPICS Archiver Appliance.

The system is configured to collect data in segments of 3 s, triggered periodically; this interval can be adjusted as needed. It also allows the user to change the number of BPM data samples acquired during each trigger cycle. All relevant machine information, such as the filling pattern, RF voltage, and measured noise characteristics, is displayed within this GUI. The noise information itself is visualized in multiple formats: as the PSD signal, prediction results, and time-series plots. This enables users to observe how the noise behavior evolves over time and to identify any correlations with changes in the machine parameters.

In addition, a separate monitoring script was developed to check the status of all BPMs. When one of the BPMs becomes unresponsive or stops updating (i.e., "hangs"), the script automatically sends a notification to the operations team via Telegram, alerting staff to investigate and resolve the issue promptly. The operating principle of the alert system is similar to that of the main alert system implemented for senior engineers in operations and maintenance. The main alert system enables engineers to promptly update the beam status whenever issues arise and is particularly important during operation and injection processes, especially in cases of beam dumps or when key parameters exceed their operational limits. This alert system, designed for the noise-monitoring system, is a separate subsystem independent of the main system. Another script is also implemented to monitor the status of PVs in the EPICS Archiver Appliance, ensuring that the data-logging process remains continuous and reliable.

3. Results and Discussion

3.1. BPMS and Data Selection

During the machine study period, all BPM cables were switched to the digital BPM system for a detailed noise analysis. To achieve an enhanced temporal resolution and data accuracy, the noise data for this study were acquired directly from the BPM processor, rather than through the BPM system integrated within the EPICS control framework. The noise patterns observed across different BPMs exhibited similar behavior, as shown in Figure 9. A dominant peak with the maximum amplitude was consistently identified at around 12.9 kHz with Vrf = 200 kV, indicating that the noise is primarily characterized by this frequency component. Among the horizontal and vertical position signals, the horizontal data displayed fluctuations more clearly, making the noise easier to detect and analyze. Consequently, the horizontal data were used for noise classification.

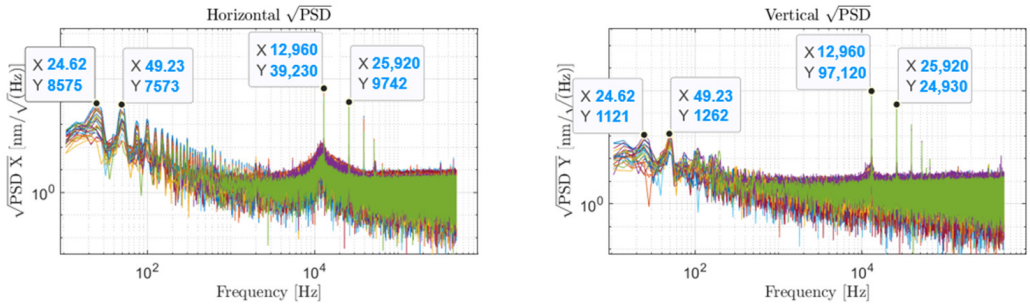


Figure 9. PSD of position data from for all 26 digital BPMs shown in different colors at RF voltage = 200 kV.

After completing the data analysis, the BPM processors were switched back to the Bergoz units to perform slow orbit feedback (SOFB) during routine machine operation. Only six BPMs positioned before and after the insertion devices were retained in the digital BPM configuration. For further study, the BPMs located upstream (BPM-MPW1) and downstream (BPM-MPW2) of the multipole wiggler were selected for a detailed analysis.

3.2. Noise Training and Testing

3.2.1. Noise Labeling

The predicted noise data, including the prediction probabilities for each class, were recorded in the archiver for future analyses. The results show the percentage of time that each noise type occurred during the beam service. However, in some cases, the system could not confidently identify the noise type when the pattern was unclear. As highlighted in Figure 10, there was noticeable confusion between the broad and multipeak classes under these conditions. This confusion arose because the noise patterns associated with the broad and multipeak classes exhibit similar spectral characteristics, making them challenging to distinguish, even through manual labeling by visual inspection.

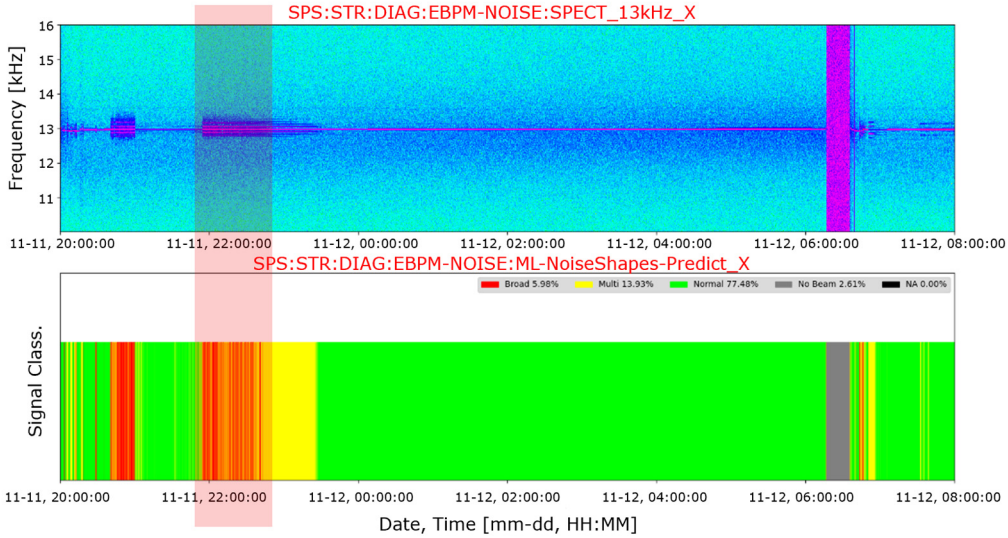
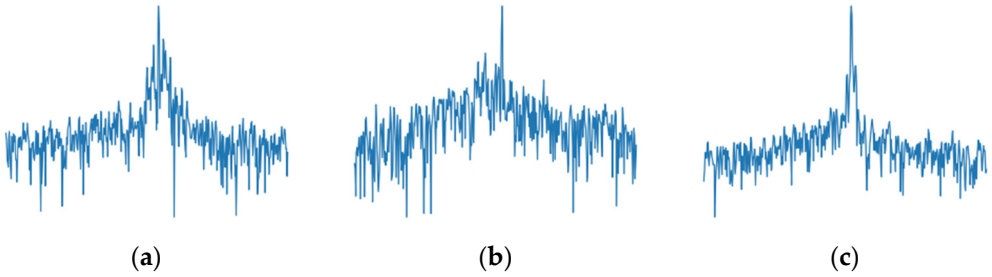


Figure 10. Noise spectrum during one operation shift with predicted noise classifications. The red highlights indicate areas of prediction confusion. Yellow represents multiple peaks, green represents a narrow peak, red represents a broad peak, and gray represents no peak.

For example, Figure 11a–c illustrate noise patterns that can be interpreted as belonging to different classes. Figure 11a can be classified either as multipeak or as having broadened frequency components. Similarly, Figure 11b could be interpreted as either a normal peak or a broad peak, depending on which part of the spectrum is emphasized; if one focuses on the baseline, it appears broad, whereas otherwise, it may be considered normal. Figure 11c is particularly ambiguous, as it exhibits a broadened frequency component at the baseline, additional side peaks, and a distinct spike at the maximum amplitude. Consequently, the signal presents characteristics that overlap among the normal, multipeak, and broad classes, making an accurate classification challenging. To address this issue, it is necessary to compare and validate the classification results against the interferogram data obtained from infrared measurements at Beamline 4.1. Further investigation is required to develop more robust methods for accurately identifying and distinguishing these overlapping noise patterns. However, overall, the predicted noise classes effectively characterize the measured data.

The recorded noise was preliminarily classified into four categories based on the available data. Other noise types may occur if the machine operates in different modes, and further data collection and investigation will be conducted during future operations. For the present study, only the four identified noise types at approximately 13 kHz are presented.



(**a**) (**b**) (**c**)

Figure 11. Examples of confusion between noise classes in the classification results: (**a**) confusion between multipeak and broad peaks, (**b**) confusion between normal and broad peaks, and (**c**) confusion among normal, multipeak, and broad peaks.

3.2.2. Model Training and Classification

Three models—TensorFlow-based 1D-CNN, PyTorch-based 1D-CNN, and MobileNetV3—were employed to evaluate and classify the noise signals. The corresponding confusion matrices and representative examples of both correct and incorrect predictions are presented in Figures 12–14. The most common source of misclassification occurred between the broad and multipeak classes, which exhibited overlapping spectral features.

The models demonstrated a perfect classification performance for the off and multipeak categories. Only two misclassifications were observed: one broad signal was incorrectly labeled as multipeak and one normal signal was misclassified as broad. These errors highlight the challenge of distinguishing between classes with subtle spectral differences, but confirm the overall robustness of the classification approach.

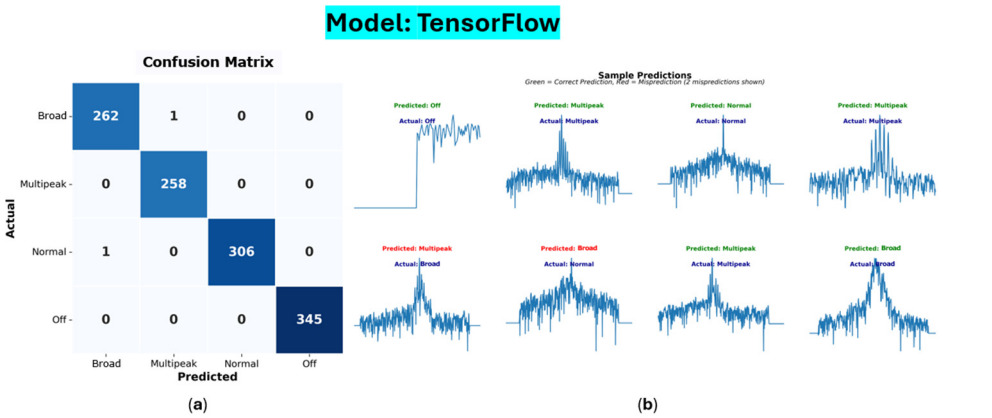


Figure 12. The confusion matrix (**a**) and sample prediction (**b**) of the TensorFlow model.

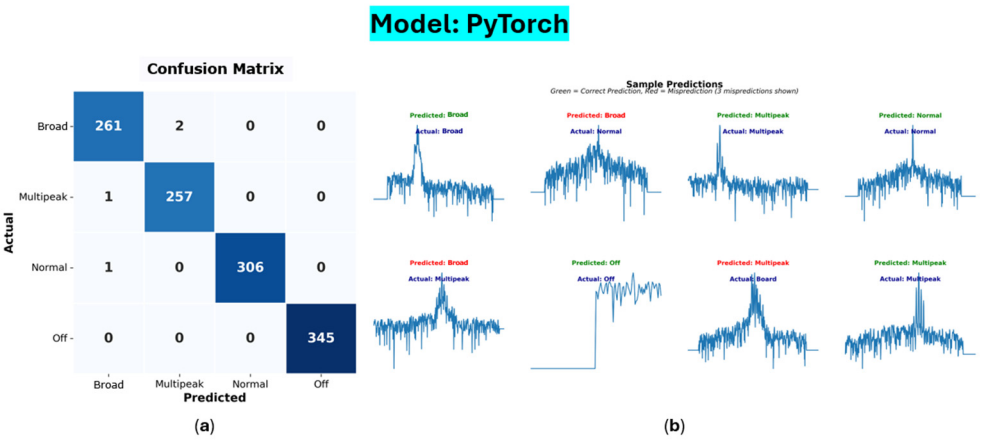


Figure 13. The confusion matrix (**a**) and sample prediction (**b**) of the PyTorch model.

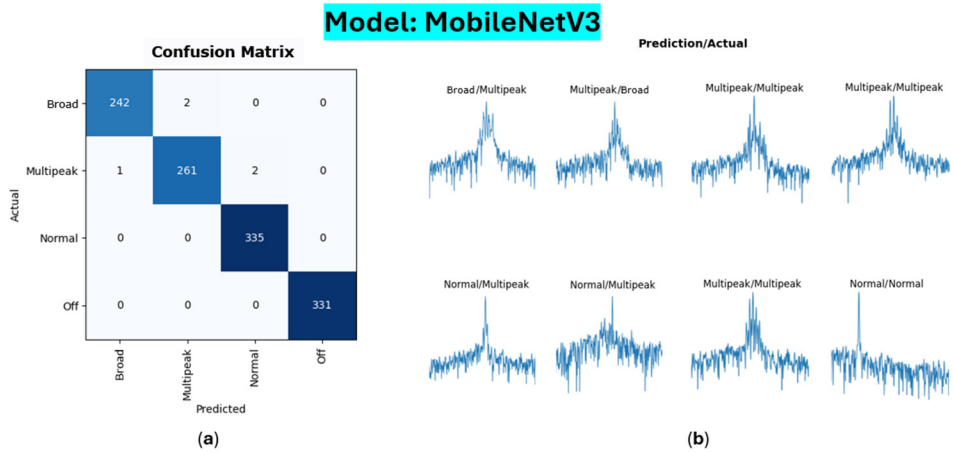


Figure 14. The confusion matrix (**a**) and sample prediction (**b**) of the Mobilenetv3 model.

As seen in Figure 15 and Table 1, a detailed performance analysis confirmed the custom 1D CNN as the most effective model, as it achieved an exceptional classification accuracy of 99.83% on the test set and correctly identified 1171 out of 1173 samples. While alternative architectures, such as the 2D MobileNetV3-based model, also demonstrated a high overall accuracy, the 1D-CNN consistently outperformed in critical classification scenarios.

A significant advantage of the 1D-CNN lies in its ability to correctly classify ambiguous or borderline cases, which are often misidentified by other models. This suggests that even a marginal improvement in the overall performance reflects a meaningful enhancement in the model's sensitivity to complex, real-world signal variations. The superior performance of the 1D-CNN can be attributed to its direct use of native, sequential spectral data, thereby avoiding the potential loss of information that may occur during transformation into 2D representations.

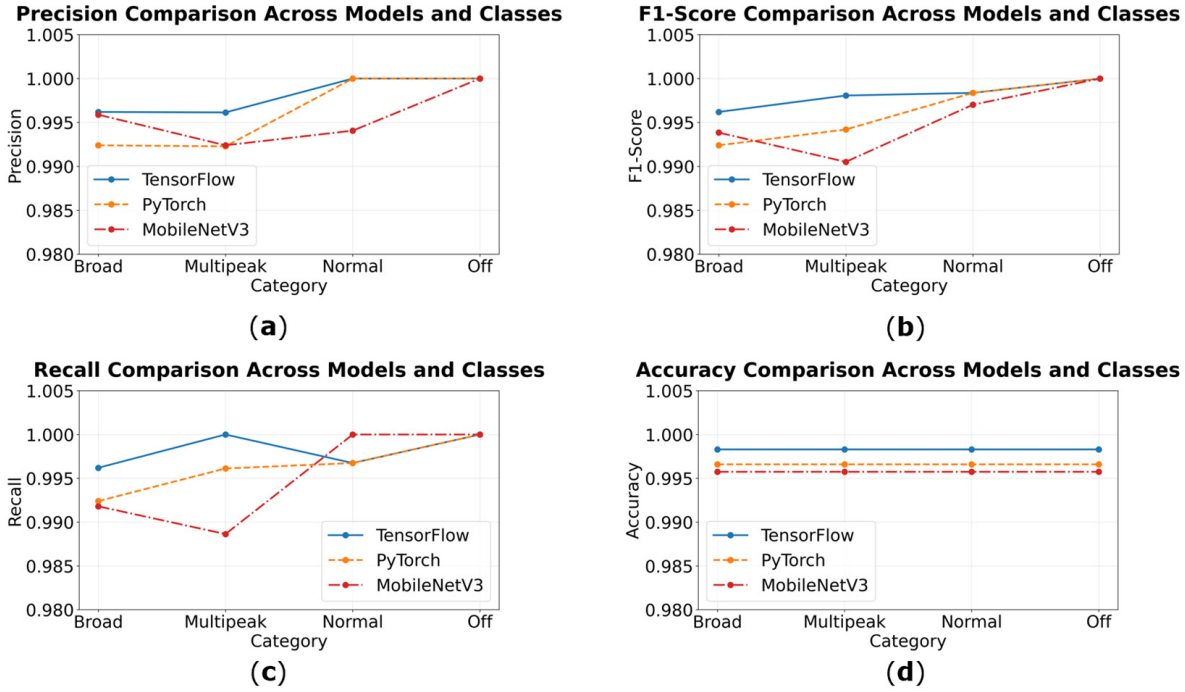


Figure 15. The (**a**) precision, (**b**) recall, (**c**) F1-score, and (**d**) accuracy of each model: TensorFlow (blue), pyTorch (orange), and MobileNetV3 (red).

Table 1. Comparison of classification results across different models and noise classes.

Models	Classes	Precision	Recall	F1-Score	Accuracy
TensorFlow	Broad	0.996198	0.996198	0.996198	0.998295
	Multipeak	0.996139	1	0.998066	0.998295
	Normal	1	0.996743	0.998369	0.998295
	Off	1	1	1	0.998295
PyTorch	Broad	0.992395	0.992395	0.992395	0.99659
	Multipeak	0.992278	0.996124	0.994197	0.99659
	Normal	1	0.996743	0.998369	0.99659
	Off	1	1	1	0.99659
MobileNetV3	Broad	0.995885	0.991803	0.99384	0.995741
	Multipeak	0.992395	0.988636	0.990512	0.995741
	Normal	0.994065	1	0.997024	0.995741
	Off	1	1	1	0.995741

One of the key challenges observed across all models is the phenomenon of "confident failure," where incorrect predictions are made with high confidence scores. This highlights the need to incorporate uncertainty estimation or confidence-aware mechanisms before deploying such models in safety-critical environments, such as accelerator control systems.

Overall, the robustness and high precision of the custom 1D-CNN make it a highly suitable candidate for real-time noise classification and beam monitoring at the Siam Photon Source. The methodologies established in this study provide a scalable foundation for further applications, including predictive maintenance and system anomaly detection throughout the facility.

3.3. System Integration: Noise-Monitoring System

CS-Studio/Phoebus was used to implement the noise-monitoring interface. The relevant parameters displayed in the application are shown in Figure 16. The blue boxes indicate the number of samples and the monitoring period, both of which can be adjusted directly within the interface. The noise patterns calculated from BPM-MPW1 and BPM-MPW2 in both the horizontal and vertical planes are also visualized. However, only the real-time prediction results for the horizontal plane are displayed within the central green circle, while the corresponding classification confidence percentages are shown as bar graphs to the right of the machine learning indicator. The color of the prediction display dynamically changes based on the identified noise type, allowing operators to immediately observe the current signal status. Additionally, time series plots below the main interface present the variation in the noise classification results over selected periods of one hour and twelve hours for each BPM. This visualization enables both the short-term and long-term monitoring of noise fluctuations, providing valuable insights for machine operation and beam quality assessments.

The system relies on precise timestamping using the internal time recorded by the BPM processor. To ensure consistency and accuracy across all components, the processor time is synchronized with the central network time protocol (NTP) server.

Additionally, a notification bot implemented in Python is used to automatically alert relevant staff via Telegram in the event of issues such as BPM connection failures, network outages, or problems archiving data. This helps to minimize data loss and maintain continuous monitoring. Furthermore, the CS-Studio/Phoebus interface has been installed in both the control room and at Beamline 4.1, providing operators and beamline scientists with real-time tools to monitor the beam performance and promptly respond to anomalies.

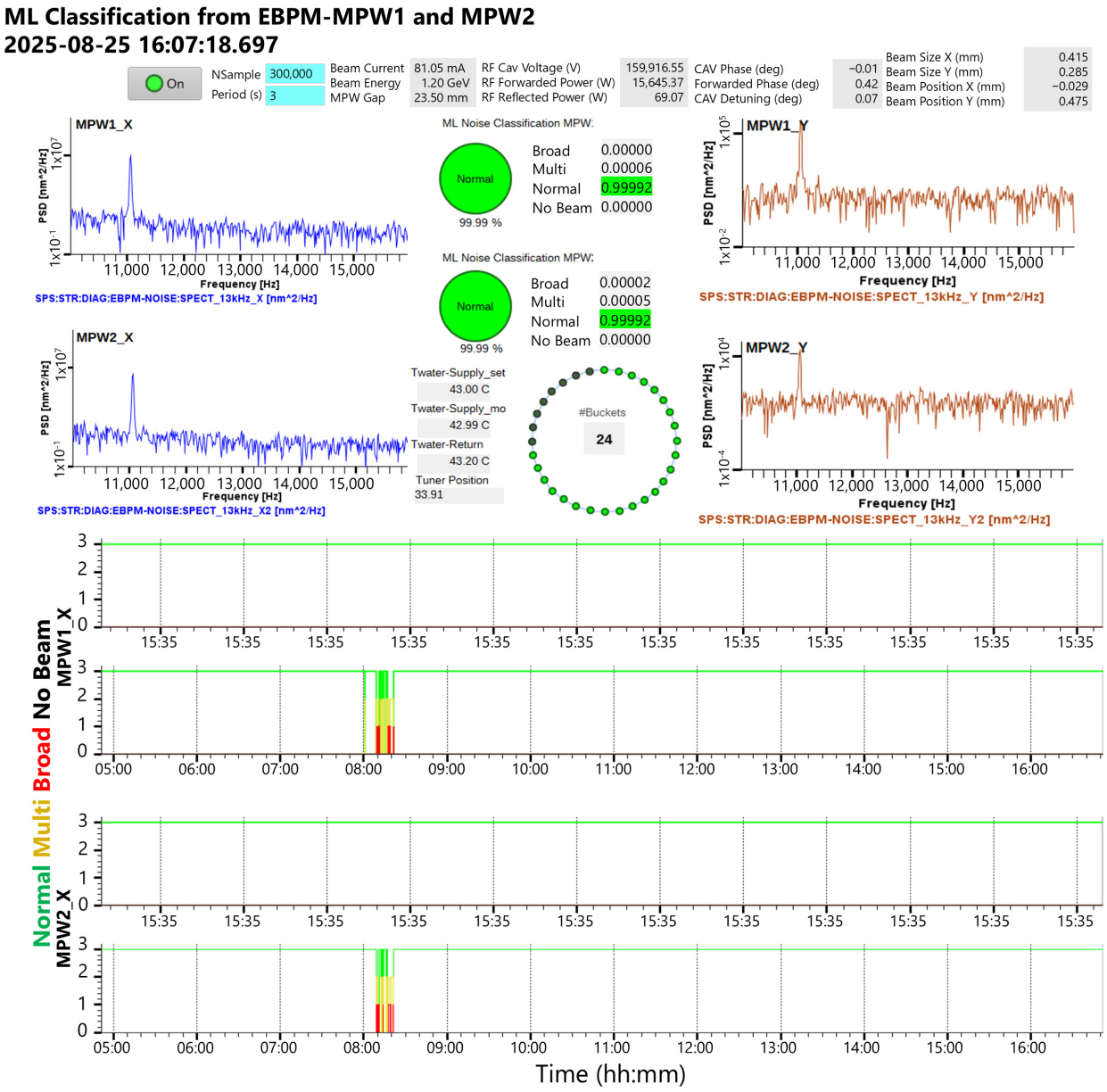


Figure 16. CS-Studio/Phoebus software for noise monitoring at Siam Photon Source.

The noise observed from the BPM can indirectly confirm the alignment of the beamline, especially in the infrared beamline. This is because the quality of the measured interferogram depends not only on the electron beam itself, but also on the optical alignment from the front end to the end station, motor control, and other components before the infrared light reaches the detector or sample. Identifying such noise helps beamline scientists narrow down the possible causes that affect experimental data. Moreover, the noise is correlated with the RF voltage, allowing us to detect fluctuations in the RF system. In addition, during operation with different operation modes (different insertion device (ID) configurations), we observed an improved beam stability when operating with all four IDs installed. This finding warrants further investigation into the underlying causes of the noise. At present, the exact cause of the noise is still under investigation. It may originate from coupled bunch instabilities or external sources such as the power supply, the RF feedback system, or the beam itself. Further investigations are planned to determine the root cause. In addition, data from other subsystems, including magnets, the RF, the vacuum, and utilities, are being recorded for future analyses.

After recording data in different operation modes, it was found that the noise around 13 kHz can be suppressed by reducing the RF voltage. Lowering the RF voltage from 200 kV to 160 kV improves the beam quality with minimal impact on the beam lifetime. Although occasional noise still occurs, it mainly appears as multipeak patterns that disappear as the beam current decreases. The remaining noise also has a narrower frequency range compared to operation at 200 kV, resulting in a more stable beam. Consequently, the RF voltage is set to 160 kV during beam service. This improved stability enhances the IR light quality, enabling smoother experimental operations at the IR beamline station.

The noise-monitoring system detects and records the beam quality in the frequency range around 13 kHz, which also affects the experimental data of the IR beamline. This monitoring assists beamline scientists in evaluating the beam quality before starting long experimental runs. Additionally, the system serves as an initial framework for beam signal monitoring, as it can be adapted to process other relevant signals of interest by changing the input data, such as the patterns of RF voltage.

4. Conclusions

In this study, a noise-monitoring system was developed and implemented to address the occurrence of beam noise observed across all beam position monitors in the storage ring at the Siam Photon Source. For practical long-term monitoring, two representative BPMs located at the multipole wiggler section, BPM-MPW1 and BPM-MPW2, were selected based on the consistent noise trends identified in their signals. Noise patterns were categorized into four classes: broad peak, multipeak, normal peak, and no beam, which were then used to train and evaluate the classification models.

The dataset was prepared in two formats: 1D numerical data and 2D images. For the 1D data, custom 1D-CNNs were implemented using both TensorFlow and PyTorch frameworks. For the 2D image data, transfer learning was applied using the MobileNetV3 architecture. The proposed system achieved an overall classification accuracy of up to 99.83 percent. These three models demonstrated the capability to accurately identify and categorize the different noise patterns with a high precision.

This implementation supports the real-time prediction and visualization of noise types, providing valuable assistance during both routine operation and dedicated machine studies. Monitoring and notification features have been integrated with Beamline 4.1 to help beamline scientists in interpreting experimental data, and deployed in the control room to support operators in maintaining beam quality during beam service.

By integrating the noise-monitoring system with the EPICS control framework and archiver log data, this approach enables a comprehensive, long-term analysis of noise sources. This monitoring strategy will be applied in future studies to investigate the origins of the observed noise, whether it originates from the electron beam itself, the RF system, or other subsystems. Ultimately, the goal is to enhance beam quality and operational stability for the benefit of users and experiments.

Author Contributions: Conceptualization, W.P., S.K. and T.P.; methodology, W.P. and S.K.; software, S.S., N.S., R.R. and P.H.; validation, S.S., S.K. and T.P.; formal analysis, W.P. and S.S.; investigation, W.P., S.K. and S.S.; resources, S.K.; data curation, W.P., S.S. and N.S.; writing—original draft preparation, W.P. and S.S.; writing—review and editing, S.K., R.R., S.J. and T.P.; visualization, W.P. and S.S.; supervision, R.R. and T.P. All authors have read and agreed to the published version of the manuscript.

Funding: This research received no external funding.

Data Availability Statement: The data that support the findings of this study are available from the corresponding author (W.P.) upon reasonable request.

Acknowledgments: The authors would like to thank the beamline scientists at Beamline 4.1: Infrared Spectroscopy and Imaging, especially the Bioimaging and Spectroscopy team, for their valuable feedback on the results and for providing a comparative analysis with the interferogram of the experimental data. Special thanks are also extended to the SPS-I operation team (SUMO and the operators) for their continuous support during the machine studies and operation.

Conflicts of Interest: The authors declare no conflicts of interest.

References

1. Klysubun, P.; Klinkhieo, S.; Kongtawong, S.; Krainara, S.; Pulampong, T.; Sudmuang, P.; Suradet, N. Beam Diagnostics at Siam Photon Source. In Proceedings of the 5th International Beam Instrumentation Conference (IBIC'16), Barcelona, Spain, 11–15 September 2016; pp. 410–412.
2. Hettel, R. Review of synchrotron beam stability and stabilizing systems. *Rev. Sci. Instrum.* **1989**, *60*, 1501–1506. [CrossRef]
3. Forck, P. Beam instrumentation and diagnostics. *arXiv* **2020**, arXiv:2009.10411.
4. USER MANUAL: Multiplexed Beam Position Monitor. Available online: https://www.bergoz.com/wp-content/uploads/MX-BPM-manual-3-0.pdf (accessed on 15 June 2023).
5. Libera Spark ERXR/ERPT. Available online: https://www.i-tech.si/products/libera-spark-erxr/ (accessed on 15 June 2023).
6. Bryant, P.J.; Johnsen, K. *The Principles of Circular Accelerators and Storage Rings*; Cambridge University Press: Cambridge, UK, 1993.
7. Dalesio, L.; Davidsaver, M.A.; Kraimer, M.R.; Hartman, S.M.; Kasemir, K.U.; Johnson, A.N.; Shen, G.; Junkes, H.; Korhonen, T.; Lange, R.; et al. EPICS 7 provides major enhancements to the EPICS toolkit. In Proceedings of the 16th International Conference on Accelerator and Large Experimental Control Systems (ICALEPCS2017), JACoW, Barcelona, Spain, 8–13 October 2017; pp. 22–26.
8. Welcome to the CS-Studio/Phoebus Documentation! Available online: https://control-system-studio.readthedocs.io/en/latest/ (accessed on 1 June 2023).
9. Nadolski, L.; Besson, J.C.; Bouvet, F.; Brunelle, P.; Cassinari, L.; Denard, J.C.; Filhol, J.-M.; Hubert, N.; Lamarre, J.-F.; Loulergue, A.; et al. Orbit stability status and improvement at soleil. In Proceedings of the 11th European Particle Accelerator Conference EPAC08, Genoa, Italy, 23–27 June 2008; pp. 3134–3136.
10. Chiu, P.; Huang, C.H.; Wu, C.Y.; Hsu, K.T.; Liao, C.Y.; Cheng, Y.S.; Hu, K.H. TPS Fast Orbit Feedback Upgrade. *J. Phys. Conf. Ser.* **2024**, *2687*, 072013. [CrossRef]
11. Bengtsson, J.; Hidaka, Y. *NSLS-II Turn-by-Turn BPM Data Analysis-A Use Case Approach*; Brookhaven National Lab. (BNL): Upton, NY, USA, 2014.
12. Howard, R.M. *Principles of Random Signal Analysis and Low Noise Design: The Power Spectral Density and Its Applications*; John Wiley & Sons: Hoboken, NJ, USA, 2004.
13. Krizhevsky, A.; Sutskever, I.; Hinton, G.E. Imagenet classification with deep convolutional neural networks. In Proceedings of the Advances in Neural Information Processing Systems 25 (NIPS 2012) Conference, Lake Tahoe, NV, USA, 3–8 December 2012.
14. Chirodea, M.C.; Novac, O.C.; Novac, C.M.; Bizon, N.; Oproescu, M.; Gordan, C.E. Comparison of tensorflow and pytorch in convolutional neural network-based applications. In Proceedings of the 2021 13th International Conference on Electronics, Computers and Artificial Intelligence (ECAI), Pitesti, Romania, 1–3 July 2021; pp. 1–6.
15. Howard, A.; Sandler, M.; Chu, G.; Chen, L.C.; Chen, B.; Tan, M.; Wang, W.; Zhu, Y.; Pang, R.; Vasudevan, V.; et al. Searching for mobilenetv3. In Proceedings of the 2019 IEEE/CVF International Conference on Computer Vision, Seoul, Republic of Korea, 27 October–2 November 2019; pp. 1314–1324.
16. Kingma, D.P.; Ba, J. Adam: A method for stochastic optimization. In Proceedings of the 3rd International Conference on Learning Representations (ICLR2015), San Diego, CA, USA, 7–9 May 2015.
17. Manasatitpong, N.S.K.; Sumano, N.; Wongprachanukul, N. SLRI EPICS Convention Discussion. 2023. Available online: https://git.slri.or.th/epics-working-group/slri-epics-management/-/blob/main/meeting/meeting_minutes_20230523.md (accessed on 24 May 2023).
18. EPICS Archiver Appliance. Available online: https://epicsarchiver.readthedocs.io/en/latest/ (accessed on 24 May 2023).

Disclaimer/Publisher's Note: The statements, opinions and data contained in all publications are solely those of the individual author(s) and contributor(s) and not of MDPI and/or the editor(s). MDPI and/or the editor(s) disclaim responsibility for any injury to people or property resulting from any ideas, methods, instructions or products referred to in the content.